Title

PHOTOELECTRON ASYMMETRIES AND TWO-ELECTRON SATELLITES NEAR THE 3p 3d GIANT-RESONANCE REGION IN ATOMIC Mn

Author

Kobrin, P.H.

Publication Date

1984-02-01

Lawrence Berkeley Laboratory
UNIVERSITY OF CALIFORNIA

Materials & Molecular Research Division

Submitted to the Journal of Electron Spectroscopy and Related Phenomena

PHOTOELECTRON ASYMMETRIES AND TWO-ELECTRON SATELLITES NEAR THE 3p → 3d GIANT-RESONANCE REGION IN ATOMIC Mn

P.H. Kobrin, U. Becker, C.M. Truesdale, D.W. Lindle, H.G. Kerkhoff, and D.A. Shirley

February 1984

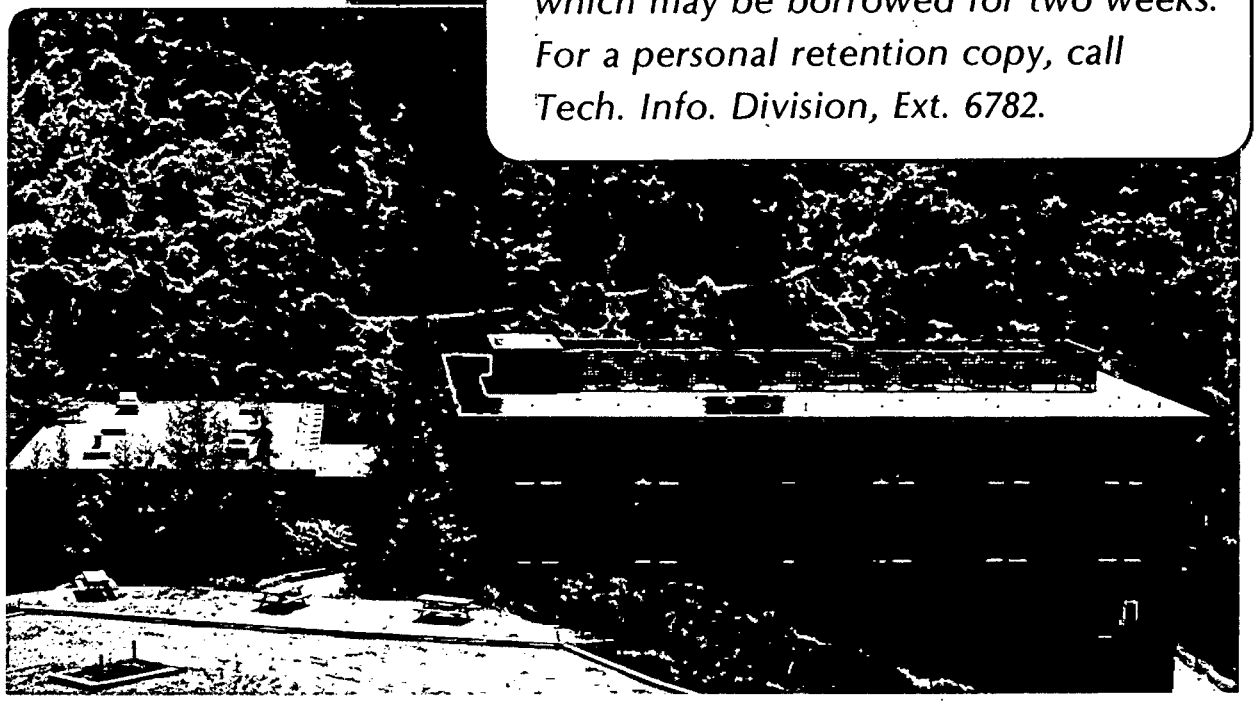

Prepared for the U.S. Department of Energy under Contract DE-AC03-76SF00098

DISCLAIMER

LBL-14545

PHOTOELECTRON ASYMMETRIES AND TWO-ELECTRON SATELLITES NEAR THE 3p → 3d GIANT-RESONANCE REGION IN ATOMIC Mn

P.H. Kobrin,* U. Becker,† C.M. Truesdale,‡ D.W. Lindle,
H.G. Kerkhoff,† and D.A. Shirley

Materials and Molecular Research Division
Lawrence Berkeley Laboratory
and
Department of Chemistry
University of California
Berkeley, California 94720

The partial cross sections and photoelectron angular distributions for several lines in atomic Mn have been measured at photon energies between 50 and 72 eV. The intensities of the 3d correlation satellites at 24–26 eV binding energy behave similarly to the main-line intensity near the 3p → 3d giant resonance, but show an enhancement near the 3p threshold which is not present for the main line. A configuration-interaction analysis is applied to help identify the origins of the satellites. The 3p/3d branching ratio from 55–72 eV and the shape of the 3d cross section in the resonance region are in good agreement with many-body perturbation-theory calculations.

*Present address: Department of Chemistry, Pennsylvania State University, University Park, PA 16802.
†Permanent address: Technische Universität Berlin, Fachbereich Physik, 1000 Berlin 12, West Germany.
‡Present address: Research and Development Division, Corning Glass Works, Corning, NY 14831.

I. INTRODUCTION

The 3p absorption spectrum of Mn I was first observed by Connerade, Mansfield and Martin [1], who found it to be dominated by a strong, broad asymmetric resonance at ~50 eV. They also reported discrete features below and above the largest resonance as well as a broad modulation in the continuum absorption immediately above the 3p threshold. They attributed the "giant resonance" to transitions from the ground state $3p^6 3d^5 4s^2\ ^6S$ to the dipole-allowed states $3p^5(3d^6\ ^5D)4s^2\ ^6P_{3/2,5/2,7/2}$. The shape and width of the resonance were explained by the mixing of the ^6P resonant states with the $3p^6 3d^4 4s^2 \varepsilon f\ ^6P$ continuum. Using Hartree-Fock calculations, they identified the lower-energy features as $3p^5 3d^6 4s^2\ ^6F$ and ^6D and the higher-energy features as $3p^5(3d^5\ ^6S)4s^2\ ^7P$ nl (nl = 4d, 5s, and 5d). The broad peak between 55 and 58 eV was identified as the maximum in the $3p^5(3d^5\ ^6S)4s^2\ ^7P\ \varepsilon s, \varepsilon d$ continua.

Davis and Feldkamp [2] applied Fano's theory [3] of the interaction of discrete and continuum states and single-configuration Hartree-Fock calculations to model the absorption spectrum. They confirmed that super-Coster-Kronig decay from the ^6P states to the $(3d)^{-1}$ continuum is responsible for the shape and width of the ^6P resonance. A higher-quality absorption spectrum [4], a many-body random-phase approximation with exchange (RPAE) calculation [5], and a many-body perturbation-theory (MBPT) calculation [6] provide further confirmation of the earlier analysis.

With resonant photoemission, it is possible to study some of the underlying details of photoabsorption. In this type of experiment, the

total cross section observed in absorption is separated into the partial cross sections for production of the different final ionic states by analyzing the energy distribution of the emitted photoelectrons.

In this paper we report the photon-energy dependence of the partial cross sections and the angular distributions for the main lines and several satellite peaks in the photoelectron spectrum of Mn. An analysis is made of the intensities of the satellite lines based on Hartree-Fock configuration-interaction (HF-CI) calculations. Of particular interest is the enhancement of the satellite intensities relative to the main 3d line at ~55 eV near the 3p threshold.

The experiment is described in Section II, and the results of our measurements are presented in Section III. Section IV contains the CI analysis of the satellites, and conclusions are summarized in Section V.

II. EXPERIMENTAL

The experiment was performed at the Stanford Synchrotron Radiation Laboratory using a grazing-incidence grasshopper monochromator with a 1200 lines/mm holographically-ruled grating, which is not usable for energies less than 50 eV. The bandpass of the monochromator was less than 0.5 eV for the spectra taken between 50 and 72 eV. A nickel grid and channeltron were used to monitor the photon intensity.

Manganese was vaporized from a resistively-heated oven similar to the one used earlier [7]. It was modified in order to reach higher temperatures, and an unheated skimmer was added to minimize the possibility of Mn coating the electron analyzers. Details of the oven are given elsewhere [8].

Spectra were taken using the double-angle time-of-flight (DATOF) method described earlier [7,9]. In brief, electrons are energy dispersed by their flight times through a 28 cm drift tube. The TOF analyzer resolution is ~3% of the electron energy, so most of the peaks in our spectra have widths of 0.7 to 1.7 eV FWHM. Analyzers placed at $\theta=0^\circ$ and $\theta=54.7^\circ$ with respect to the polarization of the synchrotron radiation are used. A peak area from the 54.7° ("magic-angle") detector is directly proportional to the photoelectron cross section, σ. The ratio of peak areas from the two detectors can be used to deduce the angular-distribution asymmetry parameter, β. This parameter completely describes the spatial distribution of the photoelectrons in the dipole approximation, for which the differential cross section is given by

$$\frac{d\sigma(\epsilon,\theta)}{d\Omega} = \frac{\sigma(\epsilon)}{4\pi}\left[1 + \beta(\epsilon)P_2(\cos\theta)\right] . \qquad (1)$$

Here, ϵ denotes the photoelectron kinetic energy and $P_2(\cos\theta)$ is the second Legendre polynomial.

The energy calibration of the analyzers was accomplished by measuring the flight times of 2s and 2p photoelectrons from neon. This also allowed for the simultaneous determination of the energy dependences of the relative transmission of each analyzer, which are used in correcting the cross-section and angular-distribution measurements.

III. MEASUREMENTS

Figure 1 shows a TOF spectrum of Mn taken at 50 eV photon energy with the 54.7° analyzer. At this energy, which lies near the maximum of the giant-resonance absorption, we observe photoelectron peaks with binding energies both below and above the main 3d line at 14.3 eV. The lines with lower binding energy are very weak except near the giant resonance, while those with higher binding energy are present in all the spectra up to 72 eV and can still be seen (as an unresolved peak) at 140 eV. The resonantly produced lines with lower binding energies are assigned as 4s peaks belonging to different couplings of the ionic configuration $3d^5 4s$. We shall refer to the group of peaks with binding energy near 21 eV as 3d* and those with binding energy near 25 eV as 3d**. Unfortunately, the Ne 2p photoelectron peak (21.6 eV binding energy) from residual calibration gas overlaps the 3d* satellites in most of our spectra.

Bruhn et al. [10] have taken photoelectron spectra over the giant-resonance region and have fitted energy profiles to the partial cross sections of the main lines. In addition, Süzer [11] has observed four peaks with binding energies greater than 20 eV in a spectrum taken at the He II resonance line energy of 40.8 eV. The energy positions of the peaks observed with binding energies greater than 20 eV are listed in Table I. The assignments of these peaks will be discussed in Section IV.

In Fig. 2 we have plotted the partial cross sections of the 3d peak and of the sum of the 4s peaks from our measurements together with the data of Bruhn et al. [10]. Points taken off resonance were used to scale

the two sets of data. Both the absorption spectrum [4], which shows a maximum split into two peaks, and the semiempirical calculation [2], which shows a low-energy shoulder, lead us to believe that the 3d partial cross-section profile results from at least two overlapping resonances. Indeed, we find that a fit of the 3d partial cross-section data to two overlapping resonances [12] (solid curve in Fig. 2) gives much better agreement than the fit to a single resonance [10]. By separating the two overlapping resonances in our fit by 0.43 eV, which corresponds to the separation of the two maxima in the absorption spectrum [4], we find an "effective" q parameter [3] of 1.6 for the larger component at lower energy, while the smaller resonance appears more Lorentzian ($q \cong 26$). Calculations using many-body perturbation theory (MBPT) suggest that the giant resonance is actually formed by a large number of overlapping resonances [6]. The 4s partial cross-section data can be equally well fitted by a single or an overlapping pair of nearly Lorentzian resonances.

We note that there is no evidence in the 3d partial cross-section data of the absorption features between 54 and 56 eV or of the small maximum in absorption between 55 and 58 eV. A plot of the cross section of the 3d** lines shows a maximum near 50 eV similar to the main 3d line and an overall decrease out to 72 eV. To look for more subtle differences, we show in Fig. 3(a) the branching ratio of this group of satellites relative to the 3d line. Because the intensities of different peaks are measured simultaneously using the TOF method, these branching ratios are independent of the corrections in photon flux and vapor pressure that were necessary to produce Fig. 2. Thus they are

intrinsically more accurate than partial cross sections. The branching ratio varies little between 50 and 54 eV, while the 3d line is changing by a factor of 3, demonstrating the similarity of the resonance behavior of the 3d** satellite lines and of the 3d main line. Between 54 and 55 eV, the branching ratio shows a sharp two-fold increase while the 3d-line intensity remains nearly constant. This sudden increase in the relative satellite intensity occurs at the same energy at which the 3p Auger line first appears in our spectra [13] and at which the absorption spectrum exhibits modulations possibly related to double-excitation processes [6]. Because the 3p electrons are difficult to detect near threshold, and because there should be an Auger electron for each 3p hole created, we have used the Auger electrons to monitor the 3p cross section. In Fig. 3(b) is plotted the branching ratio of the 3p Auger line relative to the 3d line. Also plotted in Fig. 3(b) is a MBPT curve of the 3p/3d branching ratio calculated by Garvin et al. [6] which is in good agreement with these measurements.

The resonance behavior of the asymmetry parameter provides information about the structure of the resonance states and their decay characteristics [7]. The asymmetry parameter of the 3d peak for $50 \leq h\nu \leq 72$ eV is shown in Fig. 4 together with the data of Krause and Carlson [14] and the MBPT curve by Garvin et al. [6]. It is approximately 0.65 over this energy range except where it rises to 0.9 at the giant resonance. A pronounced change in β occurs below 50 eV where the ϵf cross section is going through a minimum. The measurements by Krause and Carlson [14] show a large decrease in β below 50 eV and good agreement with our

measurements above 50 eV. For the weak 3d** peaks, the β values show too much scatter to derive reliable values, but β tends to be below one.

The resonantly produced 4s satellites have a β value of 2.0(2). To obtain $\beta < 2$ would require large spin-orbit interactions in the discrete resonance state or in the continuum channels. Provided that the remaining s electron and the outgoing p-wave are coupled to a singlet, with very little triplet mixing, we would expect $\beta = 2$, showing that parity-favored transitions are dominant [15].

IV. CALCULATIONS

In order to identify the nonresonantly produced peaks with binding energies greater than 20 eV (see Table I), we have performed Hartree-Fock configuration-interaction (HF-CI) calculations on the Mn II ion. These calculations were done with the HF code of Froese-Fischer [16], as modified by Cowan and Mann [17]. All energies have been referenced to the binding energy of the $3d^4 4s^2\ ^5D$ state (14.26 eV) [18]. From comparisons with observed states of lower binding energy, we expect these calculated energies to be accurate to within ~0.3 eV.

With up to three open subshells for some configurations, the number of possible states in Mn II is quite large. In order to limit these, we examined the "spectator model" for the 3d electrons. With all of the ionic states under consideration having four 3d electrons, the spectator model assumes that the 3d electrons will remain coupled as ^5D. Table II lists the HF energies of the possible $3d^4 4s^2$ states. There is evidence in this work and in Ref. 10 for peaks between 15 and 20 eV binding energy near the "giant resonance", but their intensities are very small above 53 eV photon energy. Thus, except in the resonance region, the spectator model appears to be valid. Therefore the remaining calculations were limited to states with a $3d^4\ ^5D$ subshell.

We then calculated energies for the states $(3d^4\ ^5D)nln'l'$ $(n,n' \leq 5)$. A further limitation of the number of states was achieved by selecting even-parity states which are coupled to a ^5D term and odd-parity states in which the outer two electrons are spin-coupled to a

singlet. The binding energies of these levels are listed in Table III. The separation into groups of odd and even parity is important when we consider the mechanisms for production of satellite peaks.

The first group of satellites, 3d*, lies at an energy that fits the assignments $(3d^4\ {}^5D)(4s4p\ {}^1P)\ {}^5P$ and ${}^5F$. These two states are listed in the tables of Corliss and Sugar [18] with binding energies of 20.6 and 20.7 eV, respectively. These authors list observed states up to the threshold for production of Mn III at 23.1 eV and therefore do not include any of the higher-binding-energy states in Table III.

Because of the uncertainties in the calculations, the satellites cannot be unequivocally assigned based on energy alone. We therefore consider the mechanisms for producing photoelectron satellite lines.

It is useful to classify photoelectron satellites, which are caused by a breakdown of the one-electron model, into three types: initial-state configuration interaction (ISCI), final-ionic-state configuration interaction (FISCI), and continuum-state configuration interaction (CSCI) [19]. These are not mutually exclusive classifications, and a given satellite may have contributions from more than one type. It is possible to look for the ISCI and FISCI contributions by doing configuration-interaction (CI) calculations on the Mn I and Mn II states. HF-CI calculations were performed with the inclusion of the main $3d^4 4s^2\ {}^5D$ final state and all of the even configurations listed in Table III. We have also done ISCI calculations with inclusion of the $3d^5 4s4d$, $3d^5 4s5s$ and $3d^5 4p^2$ configurations as well as the $3d^5 4s^2\ {}^6S$ ground state. The only appreciable mixing in these

calculations ($\geq$0.1%) was with the $3d^5 4p^2\ ^6S$ neutral state (5%) and with the $3d^4 4p^2\ ^5D$ ionic state (1%). We therefore would expect a $3d^4 4p^2\ ^5D$ photoelectron peak with an intensity on the order of 5% of the main $3d^4 4s^2\ ^5D$ line. This would account very well for one of the 3d** peaks, but the calculated energy is at least 0.6 eV too high. A calculation of an analogous satellite in Cu provides contrasting results [20]. Using shake theory, the $3d^9 5s$ satellite in Cu was calculated to have 6% of the intensity of the $3d^9 4s$ main line. Unfortunately, this peak overlaps the $3d^8 4s4p$ peak in the Cu photoelectron spectrum [21], thus this result has not been confirmed experimentally.

None of the odd-parity states in Table III can mix with the even-parity $3d^4 4s^2\ ^5D$ state, nor can their corresponding odd-parity neutral states mix with the even-parity ground state $3d^5 4s^2\ ^6S$. Production of such a satellite must therefore occur in the continuum state while the ejected electron is still present (CSCI).

Such continuum effects are more difficult to calculate. One example of such a calculation was given by Davis and Feldkamp [20]. They estimated the intensity of the $3d^9 4p$ satellite relative to the $3d^9 4s$ main line in Cu^+. They refer to this continuum-state mixing as inelastic scattering. It has also been described as "conjugate shake-up". In the Davis-Feldkamp picture, the outgoing electron inelastically scatters off the ion from which it is being ejected:

$$\begin{aligned} Cu^+:\ 3d^9 4s\varepsilon f &\rightarrow 3d^9 4p\varepsilon' d \\ &\rightarrow 3d^9 4p\varepsilon' g\ . \end{aligned} \qquad (2)$$

Davis and Feldkamp modeled this process using Hartree-Slater wavefunctions and found a $3d^9 4p$ intensity 6% of the intensity of the $3d^9 4s$ main line.

The $3d^4 4s4p$ and $3d^4 4s5p$ states in Mn^+ could be produced by a process analogous to Eq. (2). To calculate the inelastic-scattering intensity, it is necessary to evaluate a complex, two-electron integral involving the continuum electrons [R^1 (ϵf, 4s; $\epsilon' d$, 4p) in Ref. 20]. By evaluating only the imaginary part of R^1, which involves real wavefunctions only, we obtain a lower bound to the inelastic-scattering intensity. Using this approximation, we calculated the imaginary parts of R^1 for the production of the $3d^9 4p$ state in Cu^+ and the $3d^4 4s4p$ and $3d^4 4s5p$ states in Mn^+ using Cowan's Hartree-plus-statistical exchange (HX) code [22]. This code has a different approximate-exchange term than Hartree-Slater. Our results are presented in Table IV.

We have no explanation for the differences between our HX results for Cu^+ and the HS results from Ref. 20. The total inelastic-peak intensity is proportional to the sum of the squares of the ϵd and ϵf terms in Table IV plus the sum of the squares of the real parts. All of the factors involving the spin and angular-momentum quantum numbers are the same for Cu^+ and Mn^+. The values in Table IV show that we may expect that the $3d^4 4s4p$ satellite in Mn^+ to be about the same intensity as the $3d^9 4p$ state in Cu^+ (~6%), while the $3d^4 4s5p$ satellite should be an order-of-magnitude smaller.

We assign the 3d satellites as follows:

1. The assignment of 3d* is $(3d^4\ ^5D)(4s4p\ ^1P)^5P$ and ^5F. This result is based on both the peak position and the inelastic-scattering intensity. No other states are in this energy range except for the $3d^4 4s^2\ ^3F$, which would require a breakdown of the spectator model.
2. There are several possibilities for the two 3d** peaks, but the only assignment which produces appreciable intensity near the 3d** energy is the ISCI-FISCI produced $(3d^4\ ^5D)4p^2\ ^5D$, which is calculated to lie 1.1 eV higher than any peak in Ref. 10 and 0.6 eV higher than any peak in Ref. 11. This state must be considered as a strong candidate, although the energy discrepancy remains a problem. Based on energy alone, other satellites, such as $(3d^4\ ^5D)4s5s\ ^5D$ and $(3d^4\ ^5D)4s4d\ ^5D$, are possible.

V. CONCLUSIONS

The partial cross sections of the 3d and 4s main lines and of the 24–26 eV binding energy two-electron satellites are all enhanced at the $3p \rightarrow 3d$ giant resonance near 55 eV photon energy. The shape of the 3d partial cross section near the giant resonance and the 3p/3d branching ratio from 55–72 eV are in good agreement with MBPT calculations.

The off-resonant photoelectron spectrum of manganese includes two-electron satellites of the $3d^4 4s^2\ ^5D$ main line. The lines at 20.7 and 20.8 eV binding energy have been identified as $(3d^4\ ^5D)(4s4p\ ^1P)\ ^5P$ and ^5F, and their intensity has been partially attributed to inelastic scattering off the primary ion. Several possible assignments have been discussed in conjunction with the satellite structure near 25 eV binding energy. The $3d^4 4p^2\ ^5D$ assignment seems likely for one of these peaks if the energy discrepancy of 0.6 eV or more can be resolved.

ACKNOWLEDGEMENTS

The authors thank T.L. Hayhurst for his help with the ab-initio calculations, S. Süzer for providing us with his unpublished results, and L.C. Davis for helpful discussions. This work was supported by the Director, Office of Energy Research, Office of Basic Energy Sciences, Chemical Sciences Division of the U.S. Department of Energy under Contract No. DE-AC03-76SF00098. It was performed at the Stanford Synchrotron Radiation Laboratory, which is supported by the NSF through the Division of Materials Research. One of us (H.G.K.) acknowledges support by a Wigner fellowship, and one of us (U.B.) acknowledges support of the Deutsche Forschungsgemeinschaft (DFG).

REFERENCES

1. J.P. Connerade, M.W.D. Mansfield, and M.A.P. Martin, Proc. R. Soc. Lond. A 350, 405 (1976).
2. L.C. Davis and L.A. Feldkamp, Phys. Rev. A 17, 2012 (1978).
3. U. Fano, Phys. Rev. 124, 1866 (1961).
4. R. Bruhn, B. Sonntag, and H.W. Wolff, Phys. Lett. 69A, 9 (1978).
5. M. Ya Amusia, V.K. Ivanov, and L.V. Chernysheva, J. Phys. B 14, L19 (1981).
6. L.J. Garvin, E.R. Brown, S.L. Carter, and H.P. Kelly J. Phys. B 16, L269 (1983).
7. P.H. Kobrin, U. Becker, S. Southworth, C.M. Truesdale, D.W. Lindle, and D.A. Shirley, Phys. Rev. A. 6, 842 (1982).
8. P.H. Kobrin, Ph.D. Thesis, University of California, Berkeley (unpublished).
9. S. Southworth, C.M. Truesdale, P.H. Kobrin, D.W. Lindle, W.D. Brewer, and D.A. Shirley, J. Chem. Phys. 76, 143 (1982).
10. R. Bruhn, E. Schmidt, H. Schröder, and B. Sonntag, Phys. Lett. 90A, 41 (1982).
11. S. Süzer, private communication.
12. B.W. Shore, Phys. Rev. 171, 43 (1968).
13. E. Schmidt, private communication, deduced Mn 3p ionization thresholds from $M_{2,3}$ Auger spectra of gaseous atoms. He reports for $3p^5 3d^5 4s^2$:

    $^7P_4$: 56.5(2) eV

    $^7P_3$: 57.1(2) eV

    $^7P_2$: 57.4(2) eV

14. M.O. Krause and T.A. Carlson, private communication.

15. D. Dill, Phys. Rev. A 7, 1976 (1973).

16. C. Froese-Fischer, Comp. Phys. Commun. 1, 151, (1969).

17. R.D. Cowan and J.B. Mann, Jr., J. Comput. Phys. 16, 160 (1974).

18. C. Corliss and J. Sugar, J. Phys. Chem. Ref. Data, 6, 1253 (1977).

19. S.T. Manson, J. Electron Spectrosc. 9, 21 (1976).

20. L.C. Davis and L.A. Feldkamp, Phys. Rev. A 24, 1862 (1981).

21. R. Bruhn, E. Schmidt, H. Schröder, and B. Sonntag, J. Phys. B 15, L441 (1982).

22. R.D. Cowan, Phys. Rev. 163, 54 (1967).

Table I. Binding energies and relative intensities of observed Mn 3d satellites.

Line	This Work[a]	Ref. 10[b]	Ref. 11[c]	Intensity[d]
3d*	....	20.6(2)	20.7	8
		20.8(2)		
3d**	24.5	24.2(2)	24.3	7
	25.5	25.0(2)	25.2	15
			25.5	7

[a]Peak positions are difficult to determine accurately because of detector resolution and time-to-energy conversion uncertainties.

[b]$h\nu$ = 50.0 eV.

[c]$h\nu$ = 40.8 eV.

[d]Ref. 11. Intensities relative to the 3d main line (= 100).

Table II. Calculated binding energies of $3d^4 4s^2$ states relative to the ^5D binding energy of 14.26 eV.[18]

State	Binding Energy (eV)
^5D	14.3
$^3F(1)$	17.0
^3G	17.3
^3D	18.1
^1F	19.7
$^3F(2)$	20.7

Table III. Calculated binding energies of $(3d^4\ ^5D)nln'l'$ states.[a]

Parity	nln'l'	Binding Energy (eV)
even	4s4d	24.4, 25.4
even	4s5s	23.6, 24.5
even	$4p^2$	26.1
odd	4s4p	20.7, 20.8
odd	4s5p	25.0, 25.1
odd	4s4f	25.5–27

[a]Additional criteria for selection of states are given in text.

Table IV. Imaginary part of two-electron integral R^1.

		This Work	Davis and Feldkamp [20]
Cu^+ $3d^9 4s\varepsilon f$	$3d^9 4p\varepsilon d$	0.165	0.080
	$3d^9 4p\varepsilon g$	-0.020	0.021
Mn^+ $3d^4 4s^2 \varepsilon f$	$3d^4 4s 4p\varepsilon d$	0.21	
	$3d^4 4s 4p\varepsilon g$	0.03	
	$3d^4 4s 5p\varepsilon d$	0.05	
	$3d^4 4s 5p\varepsilon g$	-0.001	

FIGURE CAPTIONS

Fig. 1 Photoelectron spectrum of Mn vapor taken at 50 eV photon energy with the 54.7° detector.

Fig. 2 Partial cross sections of the 3d (circles) and 4s (diamonds) main lines from this work (filled symbols) and from Bruhn et al. (open symbols), Ref. 10. The solid curves are fits to two overlapping resonances.

Fig. 3 The branching ratios of the (a) 3d** and (b) 3p Auger lines to the 3d main line. The solid curve in panel (b) is from the MBPT calculation of Garvin et al., Ref. 6.

Fig. 4 Angular-distribution asymmetry parameter of the 3d main line from this work (filled circles) and from Krause and Carlson (X), Ref. 14. The solid curve represents a MBPT calculation by Garvin et al., Ref. 6. The dotted curve indicates a region containing many narrow closely-spaced resonances in the MBPT curve. The theoretical curve extends to 1.8 and -0.9 at its maximum and minimum, respectively.

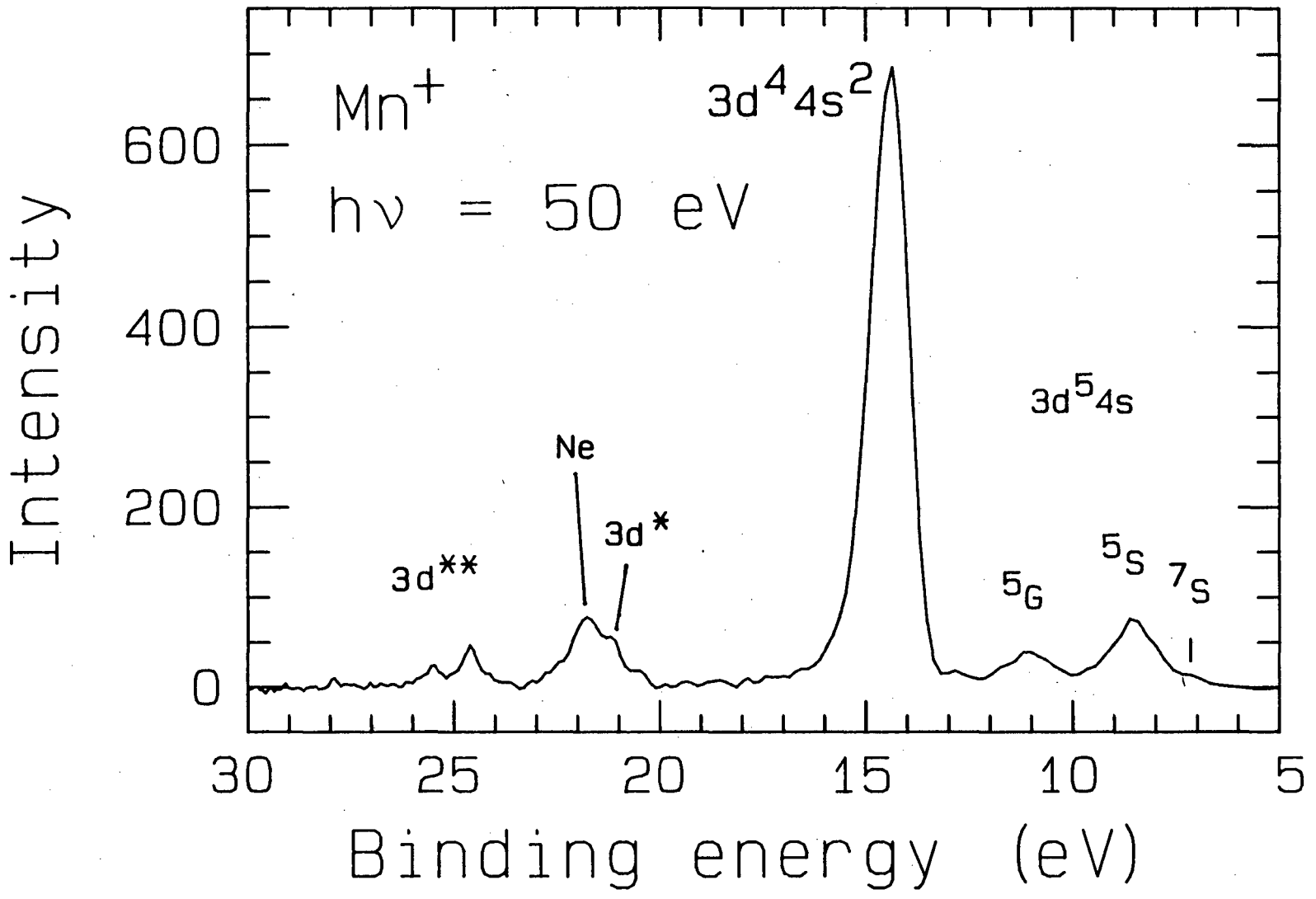

XBL 832-7859

Figure 1

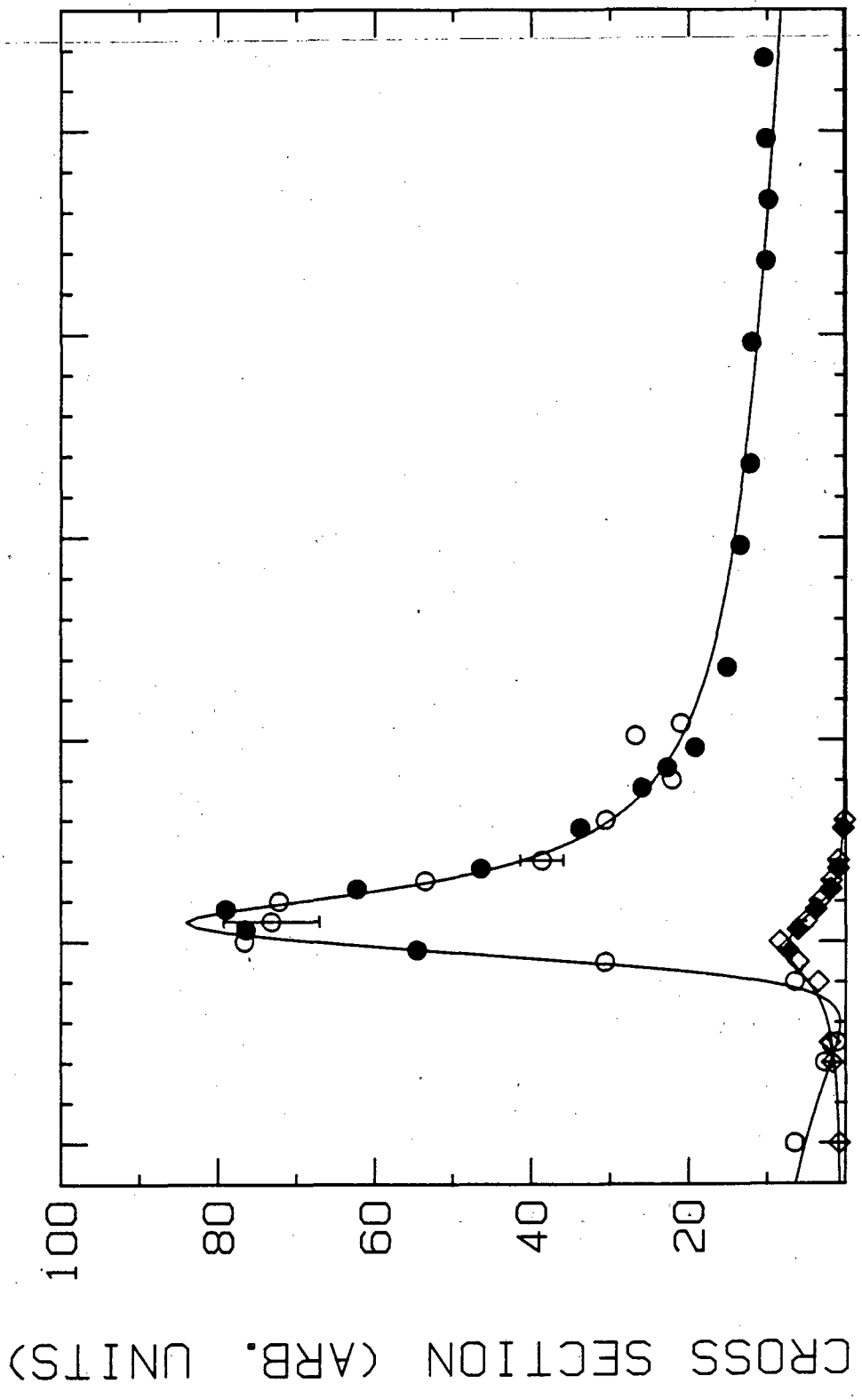

XBL 832-12211

Figure 2

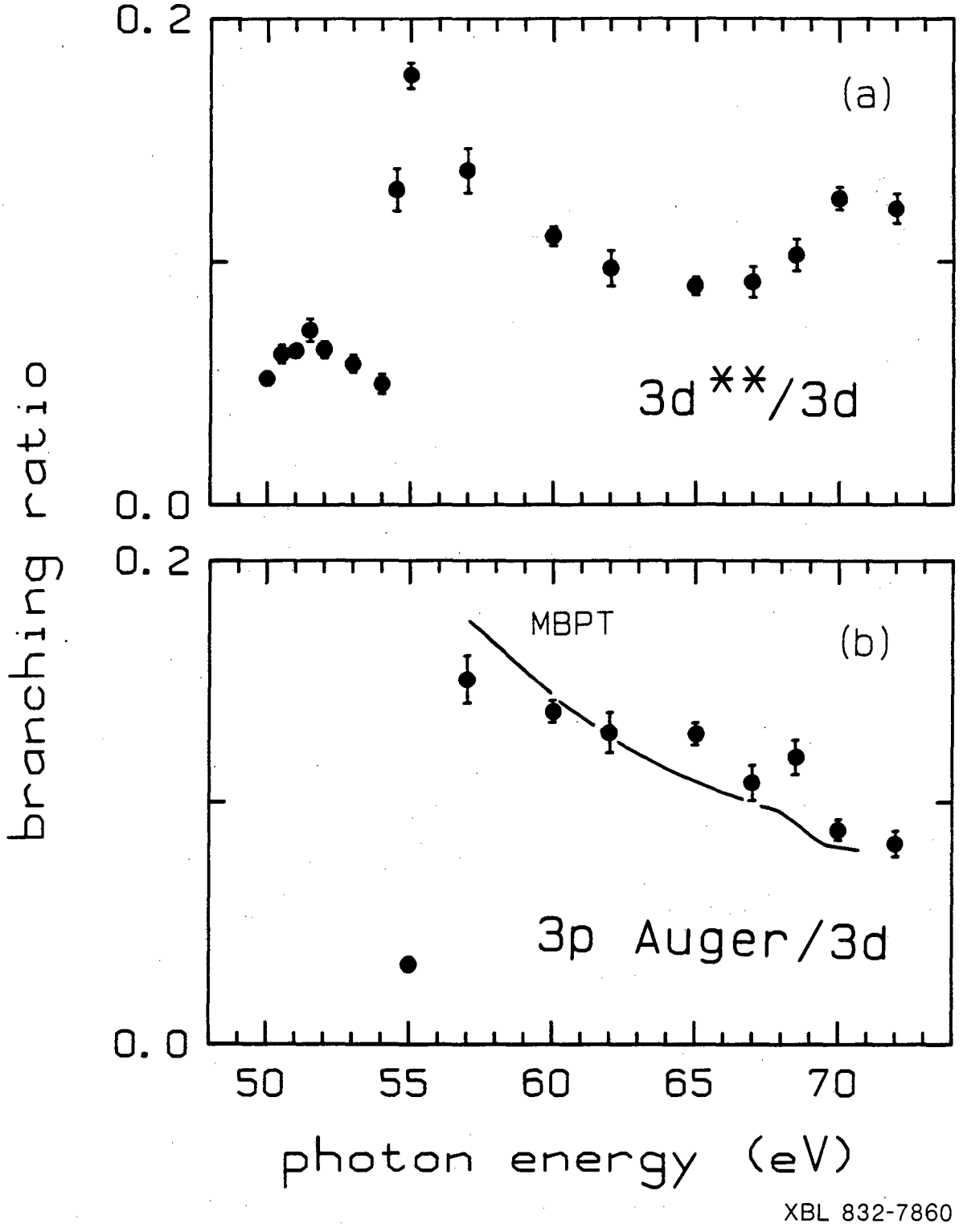
0.2
0.0
(a)
3d**/3d
0.2
0.0
MBPT
(b)
3p Auger/3d
branching ratio
50
55
60
65
70
photon energy (eV)
XBL 832-7860

Figure 3

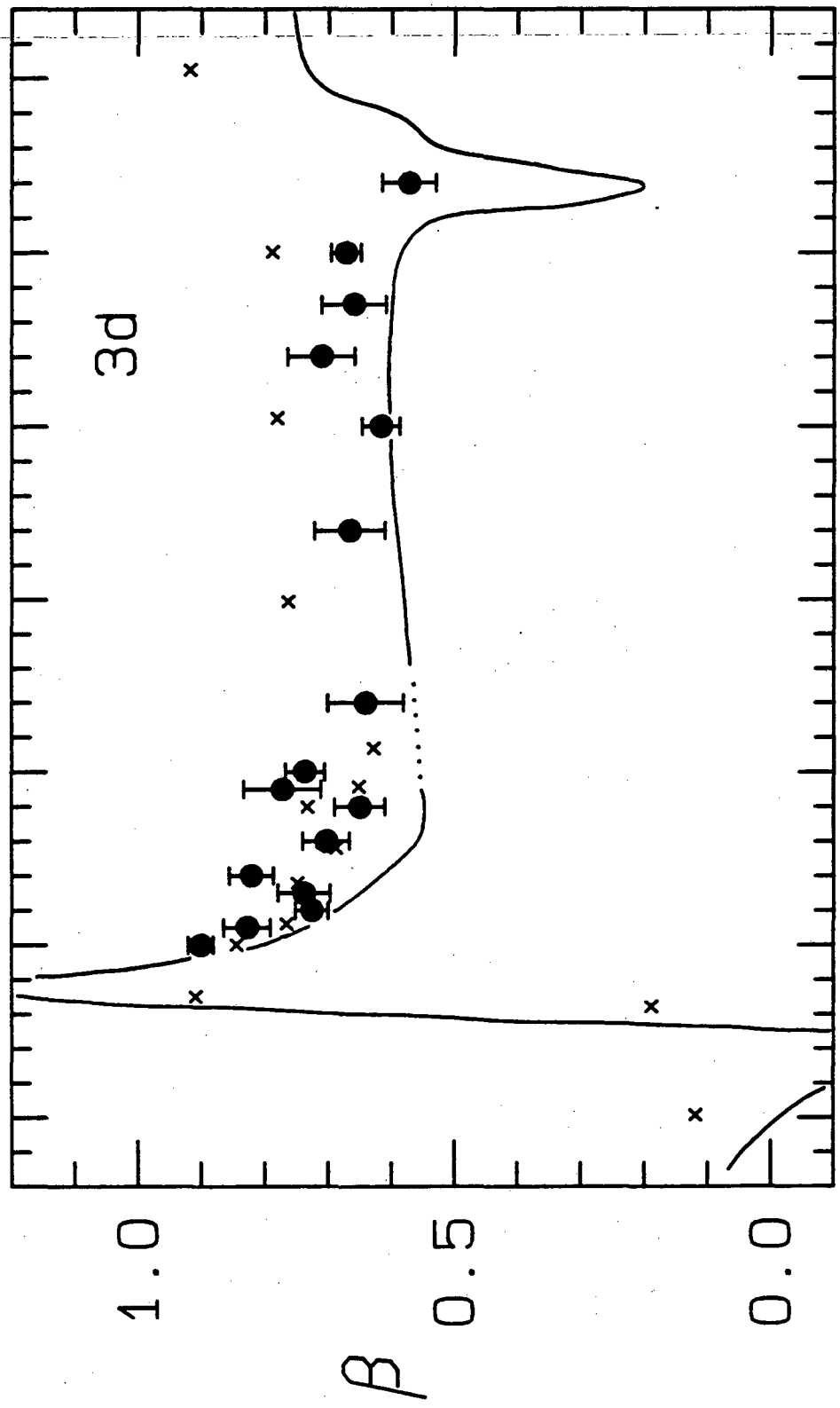

XBL 831-7656

Figure 4

This report was done with support from the Department of Energy. Any conclusions or opinions expressed in this report represent solely those of the author(s) and not necessarily those of The Regents of the University of California, the Lawrence Berkeley Laboratory or the Department of Energy.

Reference to a company or product name does not imply approval or recommendation of the product by the University of California or the U.S. Department of Energy to the exclusion of others that may be suitable.

TECHNICAL INFORMATION DEPARTMENT
LAWRENCE BERKELEY LABORATORY
UNIVERSITY OF CALIFORNIA
BERKELEY, CALIFORNIA 94720